

# Introduction to convection in porous media

Emma Lepinay \*

## 1 Introduction

The following lecture notes give a brief overview on porous media convection. A sufficient knowledge of convection is required to enjoy the following pages although the following refresher may be sufficient.

### *1.1 Overview of convection*

Convection induces a flow of fluid particles, often driven by density differences, transporting thermal energy. The density difference  $\Delta\rho$  must be sufficiently large for the onset of convection. For very large differences, the strength of convection grows and non-linear spatiotemporally chaotic motion may be observed.

A simple case of Rayleigh-Benard convection is found in the ‘two-sided’ cell problem. A sufficiently large density difference  $\Delta\rho$  between the top and bottom boundary induces a convective flow which eventually attains a statistically steady state. A ‘one-sided’ case, with  $\rho = \rho_0 + \Delta\rho$  imposed at a single boundary, can also produce an evolving convective flow, although this problem will never reach a steady state.

For example, heating a pan of cold water on the stove induces convection. Thermal energy is transferred into the cell, in this case water, via diffusion through the bottom of the pan. After some time, the water in contact with the pan becomes

---

Emma Lepinay  
Institute of Energy and Environmental Flows, University of Cambridge, UK  
e-mail: el547@cam.ac.uk

\* These lecture notes are based on the series of lectures delivered by A/Prof. Duncan Hewitt (DAMTP, University of Cambridge) at the Matrix Workshop *Instabilities in Porous Media*, April 3-23, 2024, who also assisted with the preparation of these notes.

hot compared to the colder water further above. Hot, less dense water under cold, denser water is unstable, and the hot water rises, which causes the colder parts to sink by convection. Convection increases the diffusive flux entering the domain as it ensures there is a large temperature difference at the boundary by circulating the colder water down.

## 2 A porous Rayleigh-Benard cell

In a porous medium, the two-sided convection problem is studied using Darcy's law (1) combined with the linear equation of state (2), the incompressibility condition (3), and the transport equation (4) [2]:

$$\vec{u} = -\frac{\kappa}{\mu}(\nabla p - \rho \vec{g}) \quad (1)$$

$$\rho = \rho_0(1 - \alpha T) \quad (2)$$

$$\vec{\nabla} \cdot \vec{u} = 0 \quad (3)$$

$$\bar{\phi} \frac{\partial T}{\partial t} + \vec{u} \cdot \vec{\nabla} T = D \nabla^2 T, \quad (4)$$

where the parameters in the equations above are defined as: velocity  $\vec{u}$ , permeability  $\kappa$ , viscosity  $\mu$ , pressure  $P$ , density  $\rho$ , gravity  $\vec{g}$ , temperature  $T$ , mean porosity  $\bar{\phi}$ , mean thermal diffusivity  $D$  and  $\alpha$  is a constant. The boundary conditions impose no vertical flow at the top and bottom boundaries:

$$\vec{u} \cdot \vec{n} = 0 \quad \text{at } z = 0, h$$

where  $h$  is the height of the cell. A density and temperature difference is also imposed between the top and bottom boundaries:

$$\rho = \rho_0 + \delta\rho \quad \text{and} \quad T = T_0 \quad \text{at } z = h,$$

$$\rho = \rho_0 \quad \text{and} \quad T = T_0 + \delta T \quad \text{at } z = 0,$$

where  $\rho_0$  and  $T_0$  are the initial density and temperature of the cell, respectively. This thermal problem assumes local equilibrium between the fluid and the solid matrix. If this is not assumed, a fifth equation is required to model the temperature of the rock matrix.

### 2.1 A 2D model

For the 2D problem, streamfunctions can be used to eliminate density from the problem. Satisfying the incompressibility condition gives

$$\vec{u} = \left( \frac{\partial \Psi}{\partial z}, -\frac{\partial \Psi}{\partial x} \right)$$

and therefore Darcy's law becomes

$$\nabla^2 \Psi = \frac{\rho_0 \alpha g \kappa}{\mu} \frac{\partial T}{\partial x}.$$

Taking the curl of this expression gives

$$\nabla \times \vec{u} = \vec{w} = \frac{\kappa g}{\mu} \left( -\frac{\partial \rho}{\partial y}, \frac{\partial \rho}{\partial x}, 0 \right) \quad (5)$$

which implies that the lateral gradients in density, called sloped isopycnals, induce vorticity  $\vec{w}$ . Note that all nonlinear complexity and time dependence comes from the transport equation.

### 2.1.1 Linear stability analysis

Assuming no flow, a conduction-only solution can be found for the temperature in the cell:

$$T = T_0 + \frac{T_0}{h}(h - z).$$

The stability of this base state can be analysed via linear stability analysis by imposing small perturbations of the form

$$T = T_{\text{base}} + \hat{T} e^{(\sigma t + ikx + imy)} \quad \text{and} \quad \Psi = \hat{\Psi} e^{(\sigma t + ikx + imy)}.$$

The solutions are unstable if the growth rate is positive  $\sigma > 0$ . This implies the marginal modes must satisfy

$$\frac{\rho_0 \alpha \Delta T g \kappa}{\mu D h} = \frac{(k^2 + m^2)^2}{k^2}$$

and that positive growth rates require

$$\text{Ra} = \frac{\rho_0 \alpha \Delta T g \kappa h}{\mu D} \geq 4\pi^2.$$

The parameter Ra is known as the (porous) Rayleigh number, the ratio of the driving density difference to the dissipating effects of viscosity and diffusion. If the above requirement is not met, that is, if  $\text{Ra} < 4\pi^2$ , then there is no onset of convection. Nondimensionalising the problem shows that Ra is the control parameter for the model.

### 2.1.2 Nusselt number vs the Rayleigh number

For  $Ra \geq 4\pi^2$ , the Nusselt number  $Nu$  can be introduced to characterise the strength of the flow by the dimensionless flux of heat through the system:

$$Nu = \left\langle \int \frac{\partial T}{\partial z} \Big|_{z=0} dx \right\rangle.$$

As seen in Fig. 1, the range of flow behaviour that the cell displays depends on the Rayleigh number and corresponding Nusselt number. As  $Ra$  increases from  $4\pi^2$ , the flow in the cell experiences steady convective rolls as shown by the numerical solution plot. This transforms into ‘dripping’ instabilities as  $Ra$  is further increased.

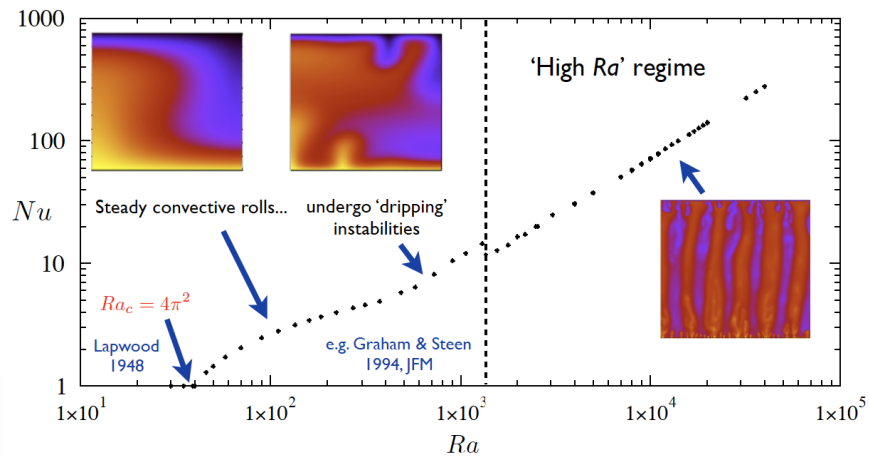


Fig. 1: The relationship between the Nusselt number  $Nu$  and the Rayleigh number  $Ra$  for a 2D porous media cell undergoing convection due to an imposed density difference between the top and bottom boundaries. The diagram highlights the range of flow behaviour that can arise due to instability [1]. For  $Ra < 4\pi^2$ , the system experiences no flow [6].

### 2.1.3 Columnar plumes

In high Rayleigh number regimes  $Ra > 10^3$ , columnar flow is observed and shown by the numerical solution in the right hand side of Fig. 1. This flow behaviour exhibits distinct channels of upward and downward motion in the interior of the cell. At the boundaries, there exists a thin diffusive boundary layer where ‘proto-plumes’ form. These grow spatially and temporally and merge to feed into the columnar

plumes. A key research area that will be explored in these lecture notes will be to understand what drives the wavelength  $k^{-1}$  of these columnar plumes [2, 3].

## 2.2 Modelling 3D cells

For a 3D porous media Rayleigh-Benard cell, a similar approach can be used to analyse the flow. Using scalar potential  $\vec{u} = \nabla \times (\nabla \times \Psi \hat{z})$ , Darcy's law can be expressed as

$$\nabla^2 \Psi = -\frac{\rho_0 \alpha g \kappa}{\mu} T.$$

The criteria for the onset of flow requires  $Ra \geq 4\pi^2$  again and a similar plot of the Nusselt number against the Rayleigh number can be constructed. The 3D model demonstrates a much broader range of flow behaviours which strongly depend on the initial conditions. For similar numerical simulations, very different flow patterns and orientations are observed. This is shown in Fig. 2, for example by comparing plot (i)  $Ra = 50$  with (i)  $Ra = 72$ . Once more, in the high  $Ra$  regime, the flow behaviour changes from clear patterns to unsteady chaotic motion.

## 2.3 High Rayleigh number regime

For high Rayleigh number regimes, where  $Ra > 10^3$ , a scaling argument can be made to predict the flux  $Nu$ . In an unconfined non-porous 2D cell, a marginally stable boundary layer argument leads to  $Nu \sim Ra^{1/3}$ . However, the asymptotic laws are still debated in the field of convection. In porous media, the same argument predicts  $Nu \sim Ra$ . Numerical experiments are in good agreement with this, although better fits exist.

### 2.3.1 Structure of columnar solutions

Numerical experiments are analysed to understand the controls on the wave number  $k$ . This parameter sets the spacing between the columns in columnar plumes and  $k^{-1}$  is the wavelength of these plumes. In the interior section of a 2D cell, the vertical advection of the background temperature gradient balances with the horizontal diffusion between the columns. The linear temperature gradient in the interior of the cell is shown in Fig. 3. As such, the cells approaches a steady 'heat-exchanger' solution given by

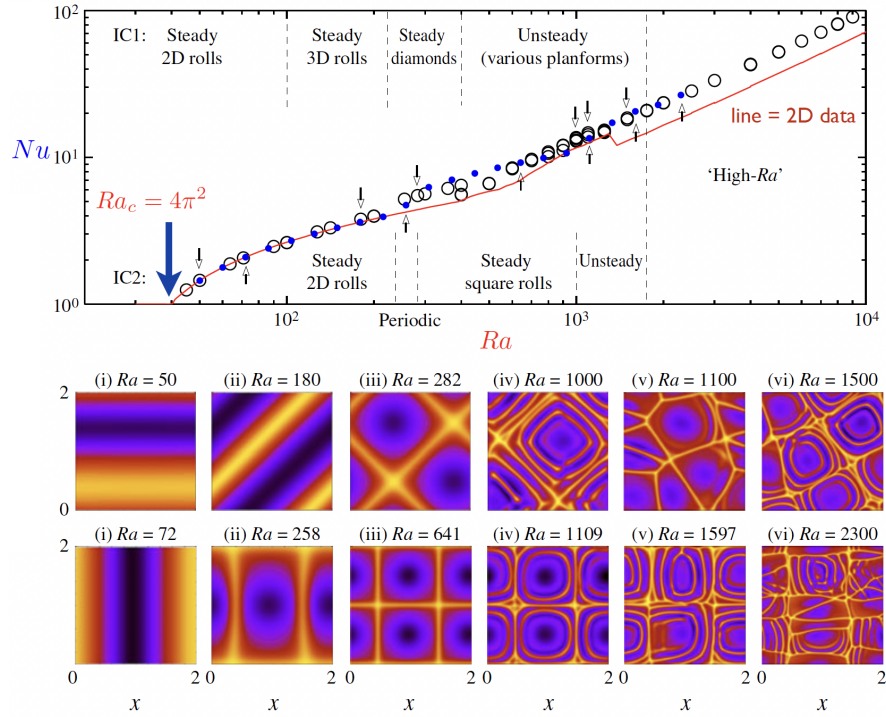


Fig. 2: The relationship between the Nusselt number  $Nu$  and the Rayleigh number  $Ra$  for a 3D porous media cell undergoing convection due to an imposed density difference between the top and bottom boundaries [5]. The black and blue circles refer to the 3D numerical simulations run and the red line shows the 2D numerical simulations. Below the plot, the numerical solutions (i)-(vi) show a slice through the mid-plane of the 3D box. The yellow sections show the strongest upward flow sections while purple sections show the strongest down-flow parts of the system. The small arrows on the plot refer to the solutions (i)-(vi). These highlight the range of flow behaviour that can arise due to instability. For  $Ra < 4\pi^2$ , the system experiences no flow.

$$T(x, z) - \frac{1}{2} = A \cos kx - \frac{k^2}{Ra} z \quad (6)$$

$$w(x, z) = A \cos kx \quad (7)$$

$$u(x, z) = 0. \quad (8)$$

Note that these solutions do not satisfy the boundary conditions.

For 3D models, cross-sections of different planes in the cells lead to similar ideas. At the top and bottom boundaries sheet-like proto-plumes are observed, while mid-

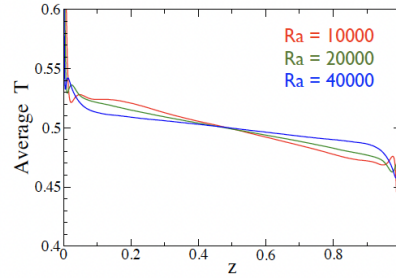


Fig. 3: The average temperature of a 2D porous Rayleigh-Benard cell against vertical position for high Rayleigh number regimes. The interior of the cell shows a linear temperature gradient.

plane snapshots indicate the presence of columnar flow. The time averaged numerical simulations are shown in Fig. 4. The cross-sections show distinct regions of upwelling and downwelling. The mechanism for these start at the boundary where ‘filamentary’ plumes develop at a very small scale. These feed in to longer lasting ‘supercells’ which themselves feed into quasi steady mega plumes in the domain. Therefore, the steady heat exchanger solution may again be used to describe the interior of the 3D cell.

$$T(x, y, z) - \frac{1}{2} = A \cos kx \cos ky - \frac{2k^2}{Ra} z \quad (9)$$

$$w(x, y, z) = A \cos kx \cos ky \quad (10)$$

$$u(x, y, z) = 0. \quad (11)$$

### 2.3.2 Relationship between the wave number and the Rayleigh number

By analysing the columnar interior plumes over long timescales, a relationship between the dominant plume spacing and the Rayleigh number can be found. Using Fourier transform and time averaging, the 2D case leads to

$$k \sim Ra^{\frac{1}{3}} \text{ to } Ra^{\frac{1}{2}}$$

whereas the 3D case has a stronger scaling of the form

$$k \sim Ra^{0.49 \pm 0.02},$$

as explored by De Paoli et al. [7]. However, at the boundaries of the cell the scaling for  $k$  is prescribed by the boundary layer such that  $k \sim Ra$ . The wave number is also limited by the advection diffusion scale from the heat exchanger equation for  $T$  such

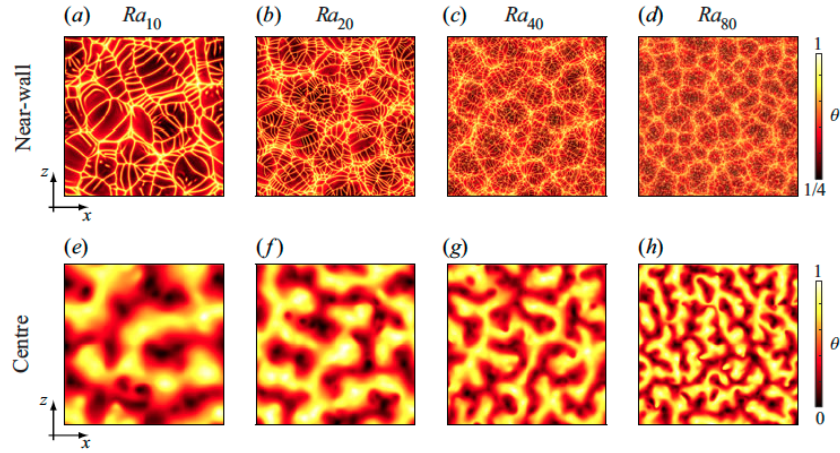


Fig. 4: Numerical simulation of temperature  $\theta$  a 3D Porous Rayleigh-Benard Box [7]. Top row: snapshot near the wall. Lower row: Time averaged cross section of the center of the 3D box.

that  $k \lesssim O(\sqrt{Ra})$ . Therefore, a question to consider is whether the stability of the interior heat-exchanger flow impacts the multiple horizontal scales associated with  $k$ , and, if so, how?

## 2.4 Stability of heat exchanger flow

Consider an unbounded heat exchanger flow in 2D. Non-dimensionalising the solutions (6)–(8) using

$$T = \frac{Ra}{k} \hat{T}, \quad u = \frac{Ra}{k} \hat{u}, \quad w = \frac{Ra}{k} \hat{w} \quad \text{and} \quad t = \frac{k^2}{Ra} \hat{t},$$

gives the base flow solution

$$T_0 = A \cos X - Z \tag{12}$$

$$w_0 = A \cos X \tag{13}$$

$$u_0 = 0 \tag{14}$$

where  $X = kx$  and  $A = \hat{A}Ra/k$ . The governing equations simplify to give

$$\nabla^2 \Psi = -\frac{\partial T}{\partial X} \quad (15)$$

$$\frac{\partial T}{\partial t} + \mathbf{u} \cdot \nabla \mathbf{T} = \nabla^2 \mathbf{T} \quad (16)$$

and, for linear stability analysis, a general solution of the form

$$\tilde{\Psi} \sim F(X) \exp \sigma t + i\alpha Z + i\beta X \quad (17)$$

$$\tilde{T} \sim G(X) \exp \sigma t + i\alpha Z + i\beta X \quad (18)$$

is used to analyse the growth rate  $\sigma$  of perturbations. Here  $\beta$  is the dominant horizontal mode number.

For a range of  $A$  values, the real part of  $\sigma$  can be found for varying  $\alpha$  and  $\beta$ . For small  $A$ , the most unstable modes are found at  $\alpha = \beta = 0$ . For  $A \gtrsim 17.5$ , the most unstable mode is found at  $\beta = 0.5$ . This implies that the system has a horizontal wavelength of 2 or twice the wavelength of the base flow. For  $A \gg 1$ , the most unstable mode has  $\Re(\sigma_{\max}) = 0.231A^{4/9}$ . Furthermore,

$$c = A = -\frac{\Im(\sigma_{\max})}{\alpha}$$

and if  $\Im(\sigma_{\max})$  is nonzero then the mode propagates at speed  $c$ . Overall the unbounded flow in this system is always unstable, which shows that there is a columnar instability. However, there is a mechanism for stability whereby columns want to coarsen and form larger ones.

#### 2.4.1 Finite domain

In a 2D finite domain, the flow is unstable to coarsening if the timescale for growth is shorter than the timescale to advect the instability across the domain. As such,

$$\frac{1}{\Re(\sigma_{\max})} < \frac{H}{c}$$

where  $H$  is the size of the domain. For  $A \gg 1$ , the theoretical stability threshold for the wave number  $k$  can be found

$$k = 1.2\text{Ra}^{5/14}$$

and any  $k$  greater than this value will produce an unstable flow.

However, the argument above does not extend to 3D. The stability of the base flow does not inform the wave number selection in a 3D cell as linear stability analysis of the base flow predicts no columnar instability.

### 3 One-sided convection

The one-sided convection problem only considers a source of buoyancy originating from a single boundary, for example, a 2D cell of depth  $H$  experiencing a dense concentration source at the upper boundary  $C(x, z, t) = 1$  while the rest of the cell has concentration  $C = 0$ . At the top boundary,  $z = 0$ , the convective flux

$$F(t) = \int \frac{\partial C}{\partial z} \Big|_{z=0} dx$$

can be calculated. The no-flux boundary condition is imposed at all other sides.

The problem can be rescaled by the buoyancy velocity  $U = \Delta\rho gk/\mu$  and the diffusion length scale  $\phi D/U$ . This simplifies the problem so that the depth of the cell becomes the only parameter, since  $H = \text{Ra}$ . Therefore, in one sided convection cells, early time dynamics have no dependence on the Rayleigh number [10].

#### 3.1 Stages of evolution of the cell

The evolution of the flux in a one sided convective cell is shown in Fig. 5. Initially, the system is started from rest, the diffusive flux  $F$  grows below the interface  $z = 0$ . Then, small fingers are observed below the interface while, in the interior, the concentration is observed to be independent of  $z$ . This marks the beginning of the instability in the boundary layer and is denoted as the linear growth region in Fig. 5.

However, as the fingers grow they start to interact and merge which causes the flux to grow. At this point the flux has a non-linear evolution. The fingers merge into descending ‘megaplumes’ which are once again fed by smaller ‘proto-plumes’ at the boundary. On this timescale, the flux is chaotic but by taking the average over the horizontal direction of the cell  $x$ , the flux is observed as roughly constant with time. After some time, shutdown is observed. The top boundary is now aware that the plumes have hit the bottom of the cell and the ambient cell fluid starts to be saturated. Further information on this process can be found in a paper by Hewitt [2].

#### 3.2 Modelling shutdown

Hewitt et al. developed a simple model which mathematically describe the process of shutdown [4]. Over a short timescale, the horizontally averaged concentration in the interior of the cell becomes uniform and independent of  $z$ :

$$\bar{C}(z, t) \approx \Theta(t).$$

The density difference evolves as  $\Delta\rho(t) = 1 - \Theta(t)$  and a simple global mass conservation leads to

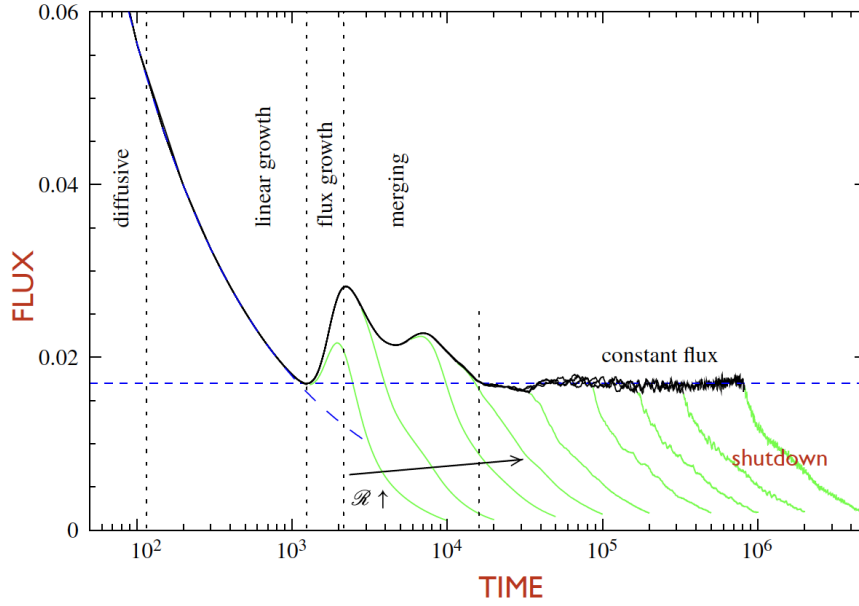


Fig. 5: The evolution of the flux in a 2D one-sided convection problem against time. Data and graph is from Slim [10].

$$\frac{d\Theta(t)}{dt} = F(t) \quad \text{and} \quad F(t) = \frac{1 - \Theta(t)}{\delta}$$

where  $\delta$  is the boundary-layer length. Therefore, assuming the boundary layer is marginally stable results in the expression

$$\delta \approx \delta_c = \frac{\alpha}{1 - \Theta(t)}$$

and hence

$$\frac{d\Theta(t)}{dt} = \alpha(1 - \Theta(t))^2$$

where the constant  $\alpha$  can be given by the 2-sided Rayleigh-Benard problem. This gives the solution

$$\Theta(t) = \frac{\alpha t}{1 + \alpha t} \quad \text{and} \quad F = \frac{\alpha}{(1 + \alpha t)^2}.$$

The wave number can be measured in the one sided convection cell by defining a time dependent local Rayleigh number at the top of the cell:  $R(t) = 4(1 - \Theta(t))Ra$ . The wave number for the one sided problem is observe to roughly match up to that of the two sided convective problem when compared.

## 4 Applications of convection in porous media

These seemingly theoretical problems have been able to increase our understanding of phenomenon observed around the world, from layered porous media to tidal heating in a planet's unconsolidated porous core.

### 4.1 Layered porous media

Horizontal layers of different porosity and permeability are often observed in geology. Increasing our understanding of the controls on fluid dynamics in the subsurface is key to analysing mechanisms such as the convective dissolution of  $\text{CO}_2$  in a relatively permeable aquifer. These can be analysed using the one-sided convective model.

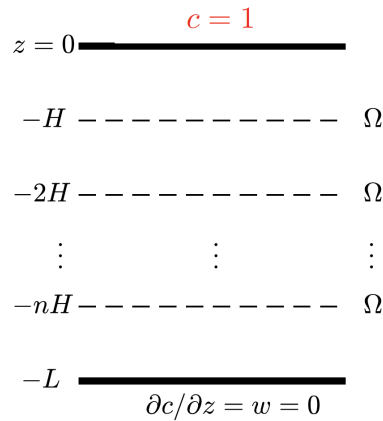


Fig. 6: Schematic of the layered porous media model. A concentration of  $c = 1$  is imposed at the top boundary while initially the rest of the porous domain has concentration  $c = 0$ . Thin layers of low permeability are equally spaced a distance  $H$  away from each other, dividing the domain horizontally. The domain has permeability  $K$  while the thin layers have permeability  $\varepsilon_k K$ .

Consider a domain of permeability  $K$  and height  $L$ . The domain is split by equally spaced, thin, horizontal, low permeability layers creating a stripe-like pattern. These have thickness  $\varepsilon_h H^*$  and permeability  $\varepsilon_k K$ . The distance between each of these thin layers is  $H$  such that there are  $n$  layers in the domain and  $L \approx nH^*$ . The porosity  $\phi$  is constant throughout the domain. At the top boundary, a density difference is imposed, for example,  $C = C_0$  at  $z = 0$  and the domain's concentration is set to  $C = 0$  initially. At the bottom boundary  $z = -L$ , the no flux boundary condition is

imposed:

$$\frac{\partial C}{\partial z} = 0.$$

The problem can again be scaled using the buoyancy velocity  $U = \rho_0 g K / \mu$  and the advection-diffusion length scale  $\Phi D / U$ . This results in a parameter-free equation with the dimensionless distance  $H$  between each layer defined as

$$H = \frac{\rho g K H^*}{\phi D \mu}$$

as shown in Fig. 6. For the thin layers, the thin low-permeability limit is considered such that

$$w = -k \left( \frac{\partial p}{\partial z} + c \right) \quad (19)$$

$$w \approx \frac{-k}{\varepsilon_h H} ([p]_-^+ + O(\varepsilon_h H)) \quad (20)$$

such that the vertical velocity is controlled by the pressure drop  $[p]_-^+$  between the top and bottom of each layer. Equation (20) implies that

$$w \rightarrow -\frac{1}{\Omega H} [p]_-^+ \quad (21)$$

for  $\varepsilon_h \ll 1$ ,  $\varepsilon_k \ll 1$  and where  $\Omega = \varepsilon_h / \varepsilon_k$  is the layer impedance. Therefore, the system is controlled by the distance between the layers  $H$ , the number of layers  $n$  and the impedance of layers  $\Omega$ .

#### 4.1.1 Numerical results as $\Omega$ changes

For  $\Omega \ll 1$ , the impedance has little effect and the system shuts down when the fingers reach the bottom of the domain. As  $\Omega$  increases, we observe a compartmentalisation and reorganisation of the plumes at each layer. For sufficiently large  $\Omega$ , the pressure drop is too small across the layer and we initially observe a shut down at the first layer with no advection across the thin low-permeability layer. Diffusive leaking across this layer can be observed which eventually, at late time, leads to an advective reorganisation. A large plume emerges and pierces through to the next layers.

## 4.2 Convection driven by an internal heat source

In unconsolidated porous cores of some planets, tidal heating can be observed. In these cases, the convection can lead to flow leaving through the top of the do-

main. As observed through numerical simulations by Le Reun and Hewitt [8], as the Rayleigh number increases, the flow changes from chaotic to steady and structured. This is shown in Fig. 7.

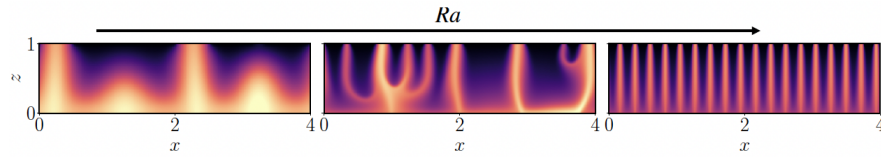


Fig. 7: Numerical analysis of porous convection driven by interval heat generation for increasing values of the Rayleigh number [8].

### 4.3 Coupled porous-fluid layer convection

Another extension to these problems is thinking about a coupled porous layer and fluid layer convection such as a Rayleigh-Benard cell with a porous medium filling the bottom half. The simulations were explored by Le Reun and Hewitt [9] and are shown in Fig. 8. In these scenarios, one question the field is investigating is whether the plumes developed in the porous media can persist within the fluid layer above, and therefore reach the top boundary.

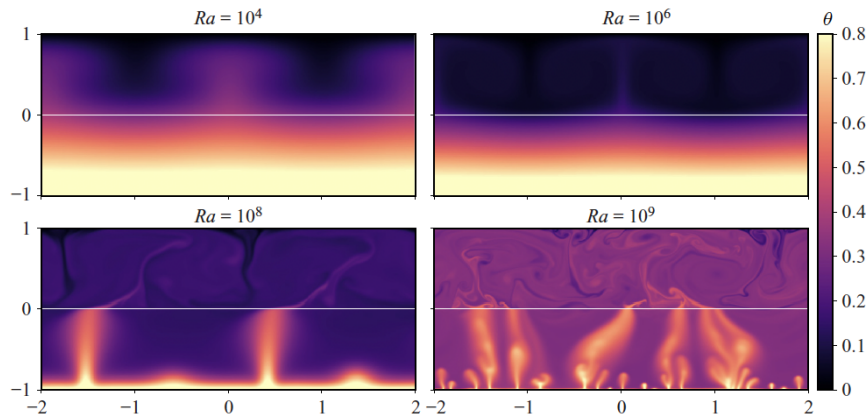


Fig. 8: Numerical analysis of a Rayleigh-Benard cell with a porous medium filling the bottom half [9]. Different cases are analysed as the Rayleigh number is increased.

## References

1. Graham, M.D., Steen, P.H.: Plume formation and resonant bifurcations in porous-media convection. *Journal of Fluid Mechanics* **272**, 67–90 (1994). DOI 10.1017/S0022112094004386.
2. Hewitt, D.R.: Vigorous convection in porous media. *Proceedings of the Royal Society A: Mathematical, Physical and Engineering Sciences* **476**, 20200111 (2020). DOI 10.1098/rspa.2020.0111.
3. Hewitt, D.R., Neufeld, J.A., Lister, J.R.: Ultimate regime of high Rayleigh number convection in a porous medium. *Physical Review Letters* **108**, 224,503 (2012). DOI 10.1103/PhysRevLett.108.224503
4. Hewitt, D.R., Neufeld, J.A., Lister, J.R.: Convective shutdown in a porous medium at high Rayleigh number. *Journal of Fluid Mechanics* **719**, 551–586 (2013). DOI 10.1017/jfm.2013.23.
5. Hewitt, D.R., Neufeld, J.A., Lister, J.R.: High Rayleigh number convection in a three-dimensional porous medium. *Journal of Fluid Mechanics* **748**, 879–895 (2014). DOI 10.1017/jfm.2014.216.
6. Lapwood, E.R.: Convection of a fluid in a porous medium. *Mathematical Proceedings of the Cambridge Philosophical Society* **44**, 508–521 (1948). DOI 10.1017/S030500410002452X.
7. Paoli, M.D., Pirozzoli, S., Zonta, F., Soldati, A.: Strong Rayleigh–Darcy convection regime in three-dimensional porous media. *Journal of Fluid Mechanics* **943**, A51 (2022). DOI 10.1017/jfm.2022.461.
8. Reun, T., Hewitt, D.: Internally heated porous convection: an idealised model for Enceladus’ hydrothermal activity *Journal of Geophysical Research: Planets* **125**, e2020JE006451 (2020). DOI 10.1029/2020JE006451
9. Reun, T.L., Hewitt, D.R.: High-Rayleigh-number convection in porous–fluid layers. *Journal of Fluid Mechanics* **920**, A35 (2021). DOI 10.1017/jfm.2021.449.
10. Slim, A.C.: Solutal-convection regimes in a two-dimensional porous medium. *Journal of Fluid Mechanics* **741**, 461–491 (2014). DOI 10.1017/jfm.2013.673.